Iraqi Journal of Physics, 2025
Vol. 23, No.2, PP. 106-117
https://doi.org/10.30723/ijp.v23i2.1340
P-ISSN: 2070-4003
E-ISSN: 2664-5548

Studying the Effect of Non-Thermal Plasma on the Structure, Optical, and Humidity Sensor Properties of Cr:Se Thin Films

Taghreed A. Hilmi[1] and Ramiz Ahmed Al-Ansari[1*]
[1]*Department of Physics, College of Science, University of Baghdad, Baghdad, Iraq*
[*]Corresponding author: ramizam_phys@csw.uobaghdad.edu.iq

Abstract

Over the past few years, there has been a significant focus on studying the synthesis and applications of metal nanoparticles. These tiny particles possess distinct properties that set them apart from bulk metals. The liquid for Cr:Se core-shell nanoparticles was made using the plasma jets method and turned into thin films that are 158.9 nm thick through chemical spray pyrolysis. The nano thin films were analyzed using X-ray diffraction (XRD), ultraviolet-visible spectroscopy, and transmission electron microscopy (TEM). This study looks at the structure and light properties of core-shell nanoparticles made with a chromium to selenium (Cr:Se) ratio of 6:4. The XRD patterns confirmed the crystalline nature of the nanoparticles for the polycrystalline ratio (6:4). When the best thin film, which is well-crystallized, is exposed to non-thermal plasma (dielectric barrier discharges (DBD)), the XRD shows important changes, suggesting it is becoming more crystalline. Tauc plots show that the direct bandgap energies change in a non-linear way, with a notable increase in energy from 2.77 to 3.88 eV. Transmission electron microscopy analysis highlights improved nanoparticle distribution and uniformity. These findings point out the importance of Cr:Se nanoparticles for advanced optoelectronic and sensing technologies, as well as various technological applications.

Article Info.

Keywords:
Cr:Se Nanoparticles, Core Shell, Surface Plasmon Resonance, Optical properties, Humidity.

Article history:
Received: Jul.09 ,2024
Revised:Nov. 04, 2024
Accepted:Nov. 8, 2024
Published:Jun.01,2025

1. Introduction

Metal nanoparticles have attracted significant attention in recent years due to their unique structural [1], optical, and electronic properties, which are highly tunable based on their composition, size, and synthesis methods [2, 3]. Among these nanoparticles, chromium-selenium (Cr:Se) nanoparticles stand out for their potential applications in optoelectronics, sensing, and catalysis [4]. The ability to manipulate their structural and electronic characteristics through controlled synthesis and post-synthesis treatments makes them promising candidates for advanced technological applications [5]. Various methods have been explored for synthesizing of chromium-selenium nanoparticles, including physical and chemical methods. Sobhani and Salavati-Niasari used a hydrothermal method with specific precursors and reducing agents [6], while Abdelouas et al. reported the use of the protein cytochrome c-3 to produce selenium nanowires [7]. Liu et al. prepared selenium nanoparticles using a reverse micro emulsion system [8]. Shin et al. synthesized selenium nanoparticles on cellulose nanocrystals [9]. These studies collectively demonstrate the potential for diverse methods in the production of chromium-selenium nanoparticles. Kuzmiak et al. [10] and Hohenester and Trugler [11] explored the surface Plasmon resonances (SPR) in metallic nanoparticles, with the former focusing on the transmittance characteristics of nanoparticles and the latter developing a method to calculate the optical properties of these particles.

Plasma is an ionization gas made up of various particles, such as positive and negative ions, electrons, atoms, molecules, radicals, and UV rays. It is commonly referred to as the fourth state of matter [12].

This study focuses on the synthesis and characterization of Cr:Se nanoparticles with different ratios of chromium to selenium (Cr:Se) of 10:0, 8:2, 6:4, and 0:10. The aim is to optimize the thin film for specific applications in optoelectronics and sensing technologies.

2. Results and Discussion

Cr:Se core-shell NPS with different Cr:Se ratios (10:0), (6:4), (8:2) and (0:10) were prepared by plasma jet. They were deposited on glass substrates using the chemical spray pyrolysis. Using the technique of plasma jet, nanoparticles were synthesized efficiently and quickly, offering numerous advantages, including low cost, environmental friendliness, and no need for expensive equipment. This was done using a DC power source with a high voltage between 20 and 25 KV, two electrodes made of stainless steel (a tube and a sheet), argon gas, and a flow meter set to 3 liters per minute. In addition, the electrodes and the air were connected to the power supply anode “terminal” and positioned 1 cm above the liquid via a stainless-steel hollow metal tube about 3 cm long, as shown in Fig. 1.

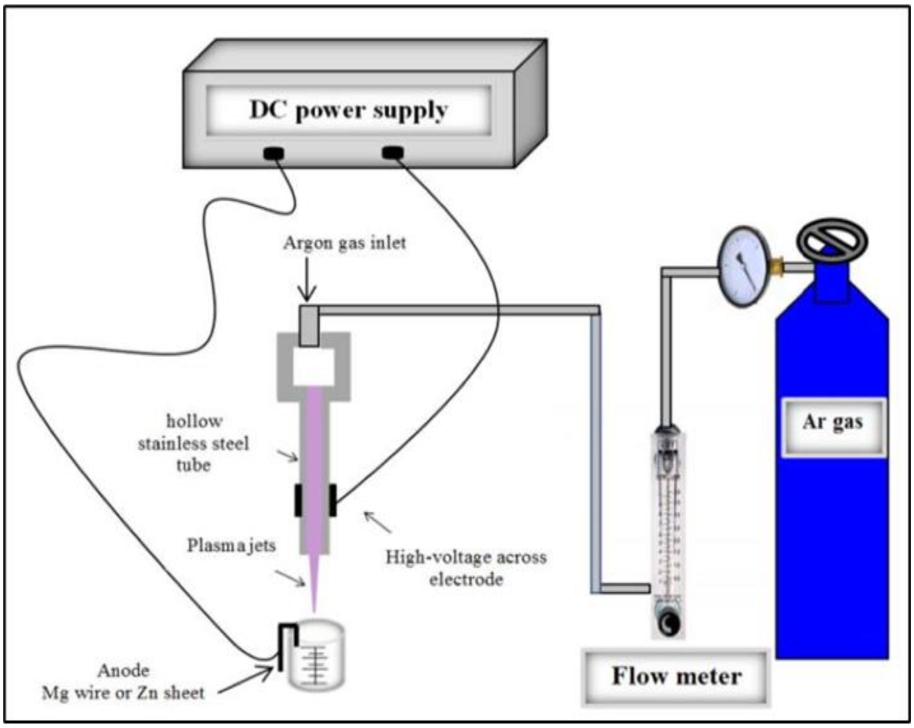

Figure 1: The Experimental setup of Cr:Se NPs synthesis by plasma jet.

The chromium solution was prepared by chromium nitrate $Cr(NO_3)_3$. Chromium nitrate of 400.15 g/mol molecular weight and 2mM concentration was added to the de-ionized water dedicated beaker, and then water was added to the beaker as a catalyst to mix chromium nitrate. To prepare selenium nitrate $SeO(NO_3)_2$ solution, a concentration of 0.5mM selenium nitrate (molecular weight of 202.98g/mol.) was added to de- ionized water dedicated beaker, and then water was added to the beaker as a catalyst to mixed selenium nitrate Eq. (1) was applied to calculating the needed weight of each chemical [13]:

$$\text{Concentration (mole)} = \frac{\text{mass}}{\text{molecular weight}\left(\frac{\text{g}}{\text{mol}}\right)\times\text{volume(liter)}} \qquad (\mathbf{1})$$

2. 1. Core Shell Synthesis

Nanoparticles with a core and a shell were synthesized in a two-step process, as shown in Fig. 2. The first stage included creating Cr NPs prepared by plasma jet for 17 min. Making the Se NPs shell that encase the Cr NPs core was the second stage. A variety of methods were used to characterize the produced Cr:Se nanoparticles.

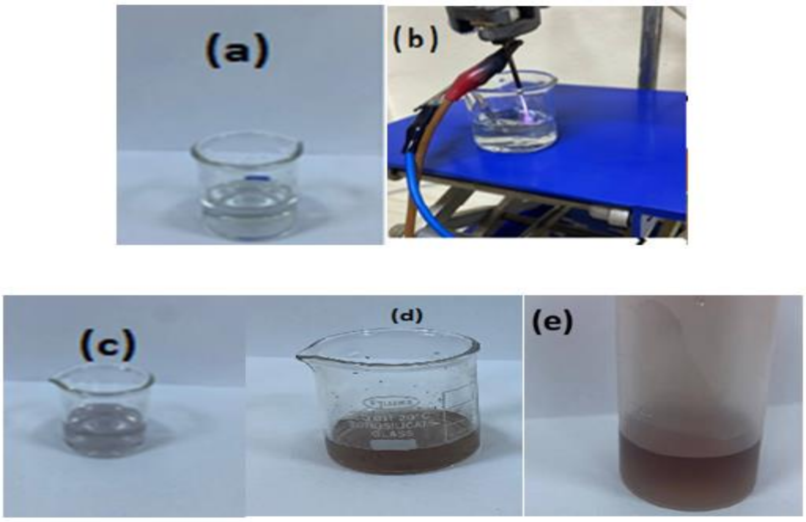

Figure 2: (a) Cr(NO$_3$)$_3$, (b) synthesis NPs by plasma jet, (c) Cr NPs (10:0), (d) Se ***liquid add to Cr NPs (e) Cr :Se NPs.***

2. 2. Deposition Thin Films

As shown in Fig. 3, Cr:Se NPs liquid was deposited on the glass substrate by the chemical spray pyrolysis method. The 2.5×2.5 cm glass substrates were first cleaned and then dried. The liquid was prepared by plasma jet system for (6:4) Cr:Se ratio. The substrates were heated with an electric heater to 275°C; a thermocouple was used to measure the temperature. A spray device was used to create the thin films. This device can control the flow of the solution by the valve of the sprayer nozzle orifice. The spray duration was 5 s, and the stop time was 55 s., the distance between the sprayer and the heater base was about 29 cm, and the air pressure was 3 bars. The films were created with good consistency.

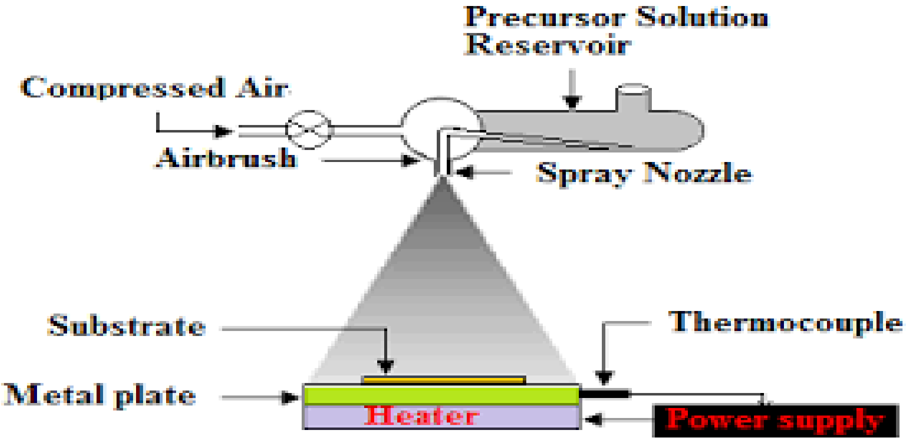

Figure 3: General schematic diagram of the spray pyrolysis deposition process.

2. 3. Dielectric Barrier Discharge (DBD) Plasma Exposure

After preparing the solution and its deposition on the substrate by chemical spray pyrolysis for Cr:Se ratio of (6:4), the structure and optical properties for core-shell thin films were studied. This was repeated after exposing the thin films to DBD plasma, as shown in Fig .4.

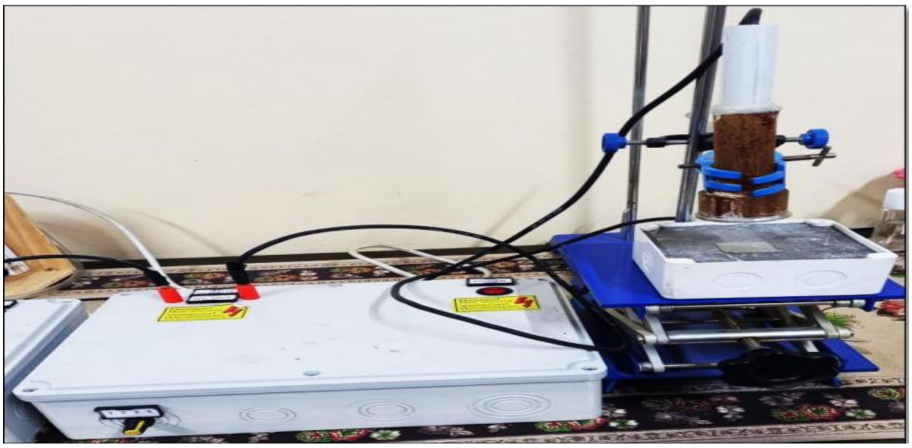

Figure 4: Designed FE-DBD system of large poles.

3. Results and Discussion

X-ray diffraction analysis was carried out to investigate the structures of Cr:Se core-shell nanoparticles thin films and determining the location of the peaks that appear to all the films according to international card (JCPDS) for (Se and Cr). Fig. 5 shows the XRD patterns of the Cr:Se core-shell nano thin films with different ratios of Cr:Se. XRD patterns revealed that the crystals in the rhombohedral structure are inclined towards a hexagonal poly crystalline arrangement. The XRD pattern for (6:4) Cr:Se NPs ratio showed that this ratio is the perfect in relation to crystalline size. The 2θ angle ranged from 10 to 80 for core and shell after and before DBD plasma, as shown in Figs.5 and 6. Before DBD, the pattern showed broad peaks of polycrystalline structure. The XRD pattern after DBD treatment exhibited sharper peaks, suggesting a transition towards a more crystalline structure. The peaks for Cr appear at 2θ = 24.48, 33.76, and 36.5 assigned to (012), (014), and (110) planes, respectively, according to (JCPDS card no. 38-1479) [14], and the peaks of Se at 2θ = 29.7°, 41.4°, and 43.7° were confirmed to be the Se-crystal planes of (101) (110), and (102), respectively, and the card no (JCPDS 98-002-2251) was paired with these peaks [15], as shown in Table 1. This comparison highlights the structural changes induced by the DBD process in Cr:Se nanoparticles thin films.

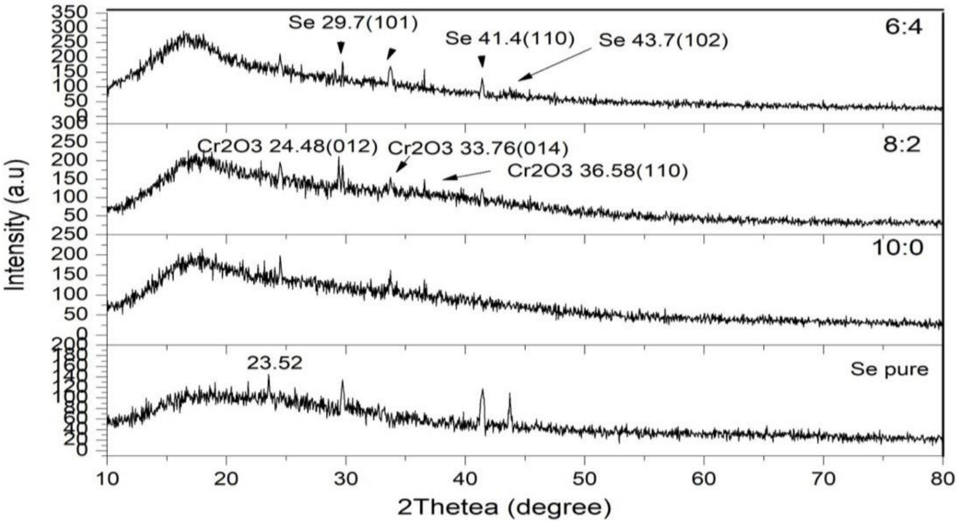

Figure 5: XRD patterns of Cr:Se nanoparticles thin film with different Cr:Se ratios (10:0, 8:2, 6:4, and 0:10).

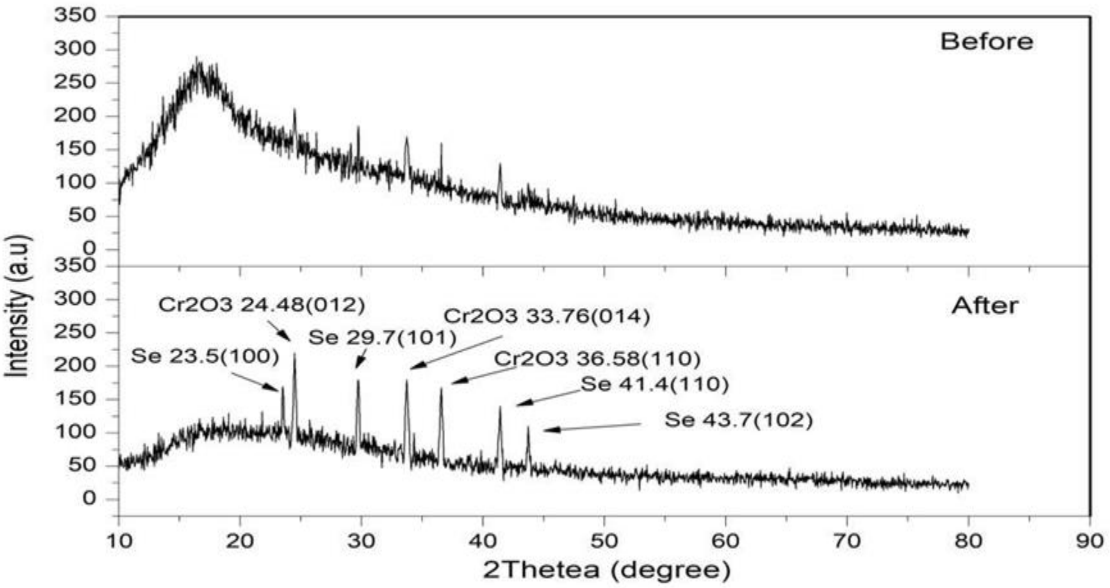

Figure 6: XRD patterns of Cr:Se thin nanoparticles film with a (6:4) ratio, before and after DBD.

The crystalline sizes were evaluated by the following Debye Scherrer 's formula [16, 17] and are given in Table 1:

$$D = \frac{K\lambda}{\beta\cos\theta} \qquad (2)$$

where: D is the crystallite size in nm, K is the Scherer's constant (0.9), λ is the X-ray wavelength in nm, and β is the full width at half maximum (FWHM) of the angles at which the peaks occur in relation to Bragg's angle in radian. The crystalline size Cr:Se nanoparticles of 6:4 was 31nm. These results show that the increase in intensity led to decrease in crystal size. These results agree well with those of Dawood et al. [18].

Table 1: The structural parameters of Cr:Se (6:4) thin films before and after DBD plasma.

Type of core-shell	phase	2θ (degree)	FWHMX (degree)	hkl	C.S (nm)	card No.
Cr:Se Before DBD	Cr_2O_3	24.48	0.219	012	38	38-1479
	Cr_2O_3	33.76	0.3237	014	26	38-1479
	Cr_2O_3	36.58	0.16716	110	52	38-1479
	Se	29.7	0.1968	101	43	98-002-2251
	Se	41.4	0.2647	110	33	98-002-2251
	Se	43.7	0.1368	102	65	98-002-2251
Cr:Se After DBD	Cr_2O_3	24.48	0.2235	012	38	38-1479
	Cr_2O_3	33.72	0.338707	014	25.61	38-1479
	Cr_2O_3	36.56	0.332	110	26.33	38-1479
	Se	2305	0.1668	100	50	98-002-2251
	Se	29.7	0.23458	101	36	98-002-2251
	Se	41.4	0.30123	110	29	98-002-2251

The TEM images provide a comparative analysis of the optimized Cr:Se nanoparticles before and after DBD treatment. In the first set of images, depicting the nanoparticles before DBD treatment, the nanoparticles appear to be aggregated with irregular shapes and varying sizes. The images (a) - (b) show clusters of particles with some degree of dispersion, but overall, the nanoparticles seem to form larger, denser clusters, indicating less uniformity and potential agglomeration. In contrast, the second set of images, taken after DBD treatment, shows a notable change in the morphology and dispersion of the nanoparticles. Post-DBD treatment, the nanoparticles are more evenly distributed and exhibit a more uniform size and shape. Images (c) - (d) reveal that the DBD treatment has resulted in a more homogeneous dispersion with fewer large aggregates. The nanoparticles appear to be better separated and more distinct, suggesting that the DBD treatment has effectively modified the surface properties of the nanoparticles. This comparative analysis indicates that DBD treatment significantly improves the morphological characteristics of Cr:Se nanoparticles, leading to enhanced dispersion and uniformity. These improvements are likely responsible for the observed increase in electrical conductivity and stability in the treated nanoparticles, as better-dispersed nanoparticles provide more effective charge transport pathways.

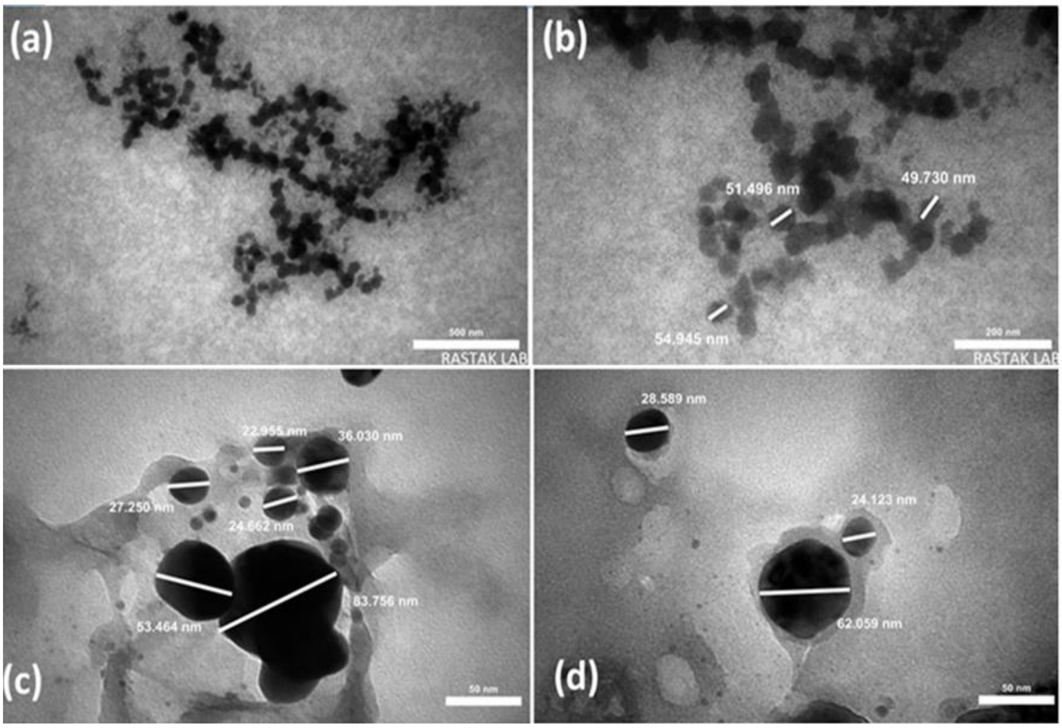

Figure 7: TEM images of the Cr:Se nanoparticles thin film a,b) before DBD c,d) after DBD treatment.

Fig. 8 shows UV-Vis absorption spectra of Cr:Se nanoparticles thin film with different Cr:Se ratios. The absorption of materials is affected by several factors, such as material type, wavelength of incident radiation and the thickness of the film [19]. Absorption was measured as a function of wavelengths based on the transmittance spectrum within the range 300-1100 nm for the Cr:Se core-shell nanoparticles films for all ratios (10:0,8:2,6:4,0:10). The results showed that the absorption was reduced as wavelength increased due to decrease of the photon energy and inability to make electrons move from the valence band to the conduction band. That is, the relationship between wavelength and photon energy is inverse. The absorption values begin to decrease after exposure to non-thermal plasma at 5s with increasing wavelength because the energy gap after DBD plasma increases, decreasing absorption, as shown in Fig. 9. Fig. 10 presents Tauc plots according to [20]:

$$\alpha h\upsilon = B_o (h\upsilon - Eg_{opt})^r \quad \textbf{(3)}$$

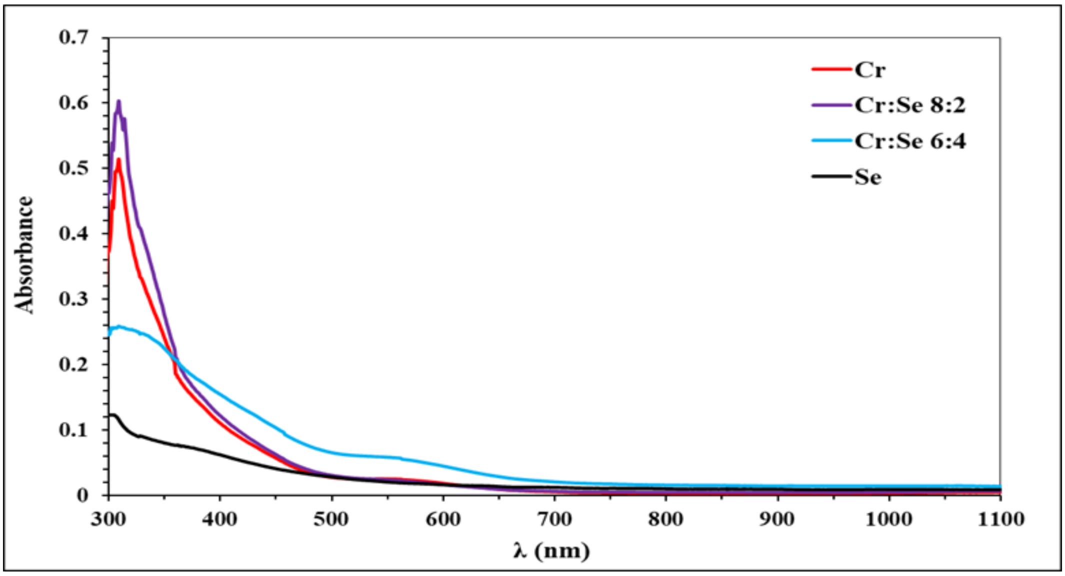

Figure 8: UV-Vis absorption spectra of Cr:Se nanoparticles thin film with different ratios.

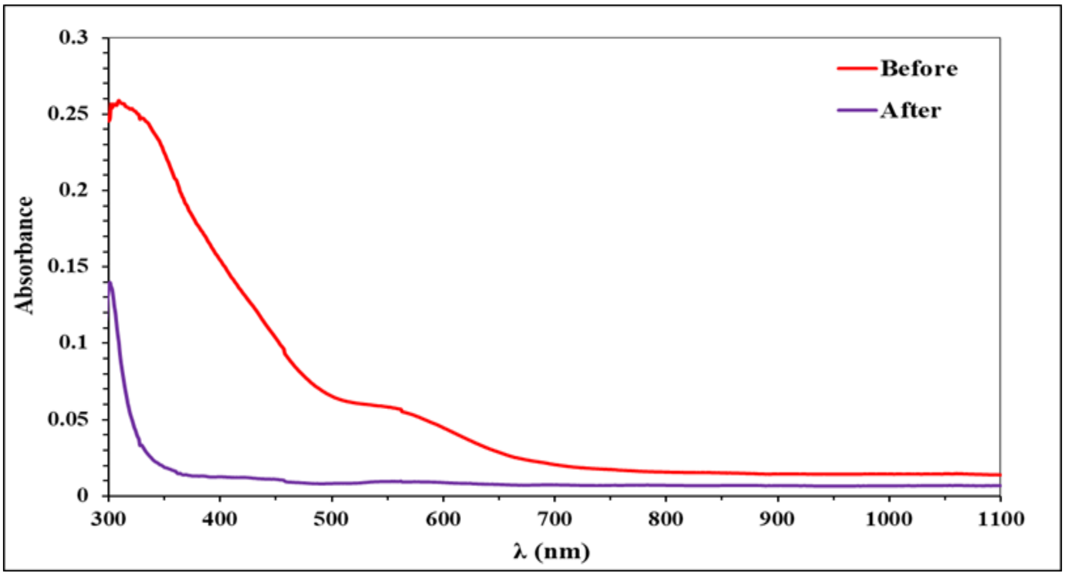

Figure 9: UV-VIS absorption spectra of (6:4) Cr:Se nanoparticles before and after DBD plasma.

where: α denotes the absorption, h is Planck's constant, υ is the incident photon frequency, B_o denotes a constant about 0.9, Eg_{opt} denotes the optical energy gap, and r is a value depends on the nature of the transition type. The direct bandgap energies of Cr:Se nanoparticles with varying ratios of (10:0), (8:2), (6:4), and (0:10) were determined from these plots. Fig. 10(a) shows the plots for Cr:Se NPs with a (10:0) ratio, exhibiting a direct bandgap energy of 3.37 eV. Fig. 10(b) illustrates the plots for NPs with (8:2) Cr:Se ratio, where the direct bandgap energy increases to 3.6 eV. Fig.10(c) is the plot of NPs with a (6:4) Cr:Se ratio, which shows a direct bandgap energy of 2.77 eV. This decrease is because of defects and the reduction in chromium, while Fig. 10(d) presents the NPs with a (0:10) Cr:Se ratio, which has a direct bandgap energy of 2.78 eV.

The optical energy gap is an important parameter in studying the properties of films and determining their possibility of using them in gas or humidity sensors. The energy gap gives a clear idea of the optical absorption. The films are transparent to radiation when the incident energy is less than the energy gap ($h\nu<E_g$), absorption occurs when

the incident radiation has a larger energy than the energy gap (hν>E_g). The Cr:Se is a semiconductor with a direct band gap. The optical energy gap for Cr:Se core-shell nanoparticles thin films deposited on glass substrates was calculated for the permissible direct electronic.

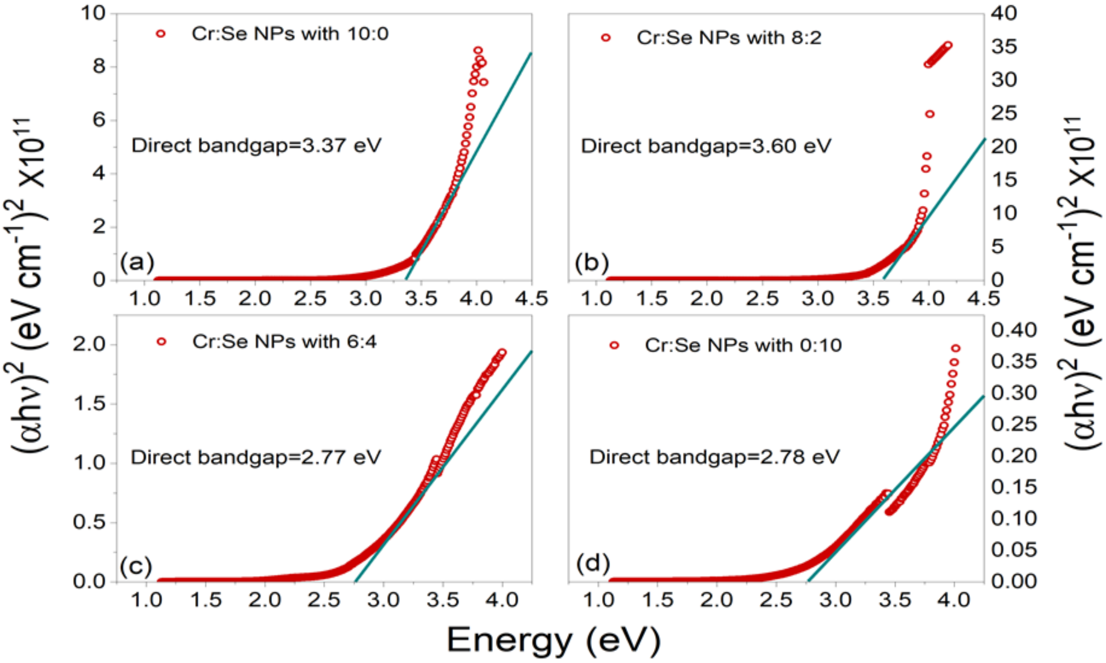

Figure 10: Tauc plots for determining the direct bandgap energies of (Cr:Se) nanoparticles thin film with different Cr:Se ratios: (a) (10:0), (b) (8:2), (c) (6:4), and (d) (0:10).

These results indicate that the bandgap energy of Cr:Se NPs is significantly influenced by the Cr:Se ratio. The bandgap decreases as the ratio moves from 10:0 to 6:4, reaching its lowest 2.77 eV, at the 6:4 ratio 2.77 eV, and then slightly increases at the 0:10 ratio 2.78 eV. This non-linear trend suggests that the electronic structure and the resultant bandgap energy of the Cr:Se NPs depend highly on the relative concentration of chromium and selenium. Specifically, higher chromium content (as in 10:0 and 8:2 ratios) results in higher bandgap energies, while increasing selenium content reduces the bandgap energy to a certain point [21]. A large bandgap generally indicates a lower intrinsic carrier concentration at room temperature, impacting the conductivity and carrier mobility of the material. In summary, the DBD treatment has resulted in a substantial increase in the direct bandgap energy of Cr:Se nanoparticles, significantly altering their electronic and optical properties and potentially improving their performance in specific technological applications, as observed in the 6:4 ratio. This could be due to changes in the crystal structure and defect states. The energy gap of Cr:Se nanoparticles of 6:4 ratio increased after exposure to non-thermal plasma at 5 s from 2.77 to 3.88 eV, as shows Fig. 11. The increase in the energy gap is due to the effect of the non-thermal plasma on the thin film causing many changes in structures, also it leads to the reduction of the impurities in the thin film.

A hygrometer is a device used to measure humidity. Hygrometers come in analog and digital versions, but modern digital hygrometers are more accurate. The resistance variation of the (Cr:Se) (6:4) sensor, before and after DBD as a function of humidity is shown in Fig. 12. It is evident for both cases, that by increasing the relative humidity (RH) from 50 to 97% RH, the resistance decreases from 29.25 to 24.86 MΩ and from 1.851 to 1.833 MΩ for as prepared and plasma treated samples. This decrease in resistance is due to the water physisorption processes on the entire porous structure of the sample surface as water layers. The increase in charge carriers and H^+ ions on the sample surface is responsible for the decrease in resistance based on Von Grotthuss mechanism. The von Grotthuss mechanism provides a detailed explanation of proton mobility in hydrogen-bonded liquids like water. The proton hopping along hydrogen-bonded chains accounts for the high proton conductivity observed in these systems [22].

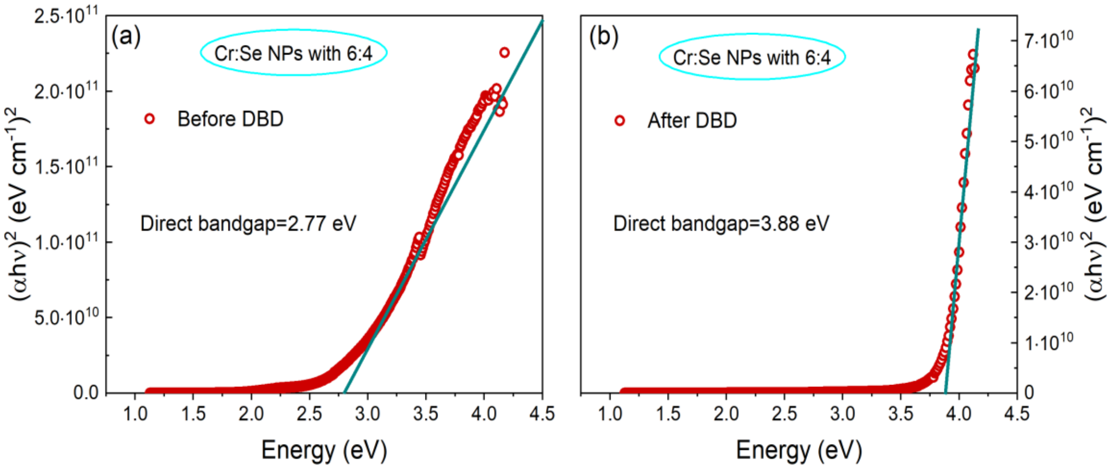

Figure 11: Energy bandgaps of Cr:Se NPs thin film with a (6:4) ratio before and after DBD plasma.

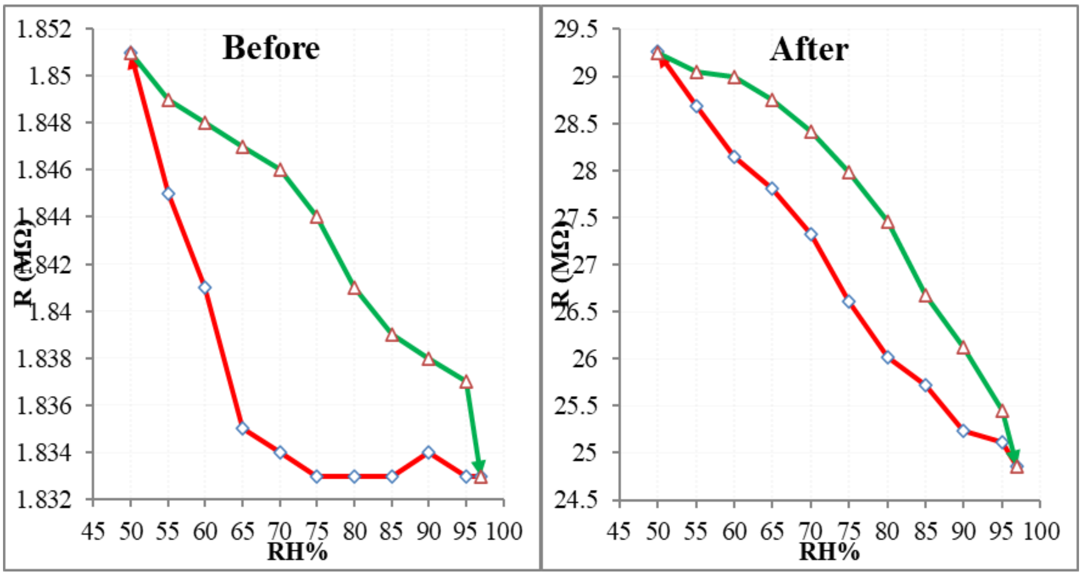

Figure 12: Relative humidity (%) of Cr:Se NPs thin film with a (6:4) ratio for both after and before DBD treatment.

The resistance of sensor does not immediately return to its original value after reducing humidity. This delay results in a hysteresis loop during adsorption and desorption cycles [23]. The rate at which water molecules adsorb and desorb from the sensor's surface varies according to the surface nature. For the plasma treated samples, the nature of the sensor surface changes significantly. Plasma treatment can modify surface hydrophobicity or hydrophilicity, which directly impacts the adsorption and desorption of water molecules, which affects how water molecules interact with the sensor's surface. A more hydrophobic surface may repel water molecules, affecting the adsorption process differently than a hydrophilic surface [24, 25]. Plasma treatment also increases the surface area and the number of active sites available for adsorption. This can enhance the initial adsorption process but also complicate the desorption, as more water molecules are trapped in these active sites. So, the final hysterias shape of the plasma treated sample is more suitable for humidity sensing [26].

The humidity sensitivity $S_{RH}\%$ was determined according to Eq.4 [27]

$$\mathrm{S_{RH}}\% = \frac{\mathrm{R_{50}}-\mathrm{R_{RH}}}{\mathrm{R_{RH}}} \times 100\% \tag{4}$$

where: R_{50} is the resistance of the sample at the started point of 50 RH humidity, and R_{RH} is the sample resistance at each RH level. The humidity sensing of the (Cr:Se) (6:4) sensor, before and after plasma exposure as function of humidity is shown in Fig. 13. It appears that the sensitivity improved from 1 to 17.7% at 97% RH after the plasma treatment.

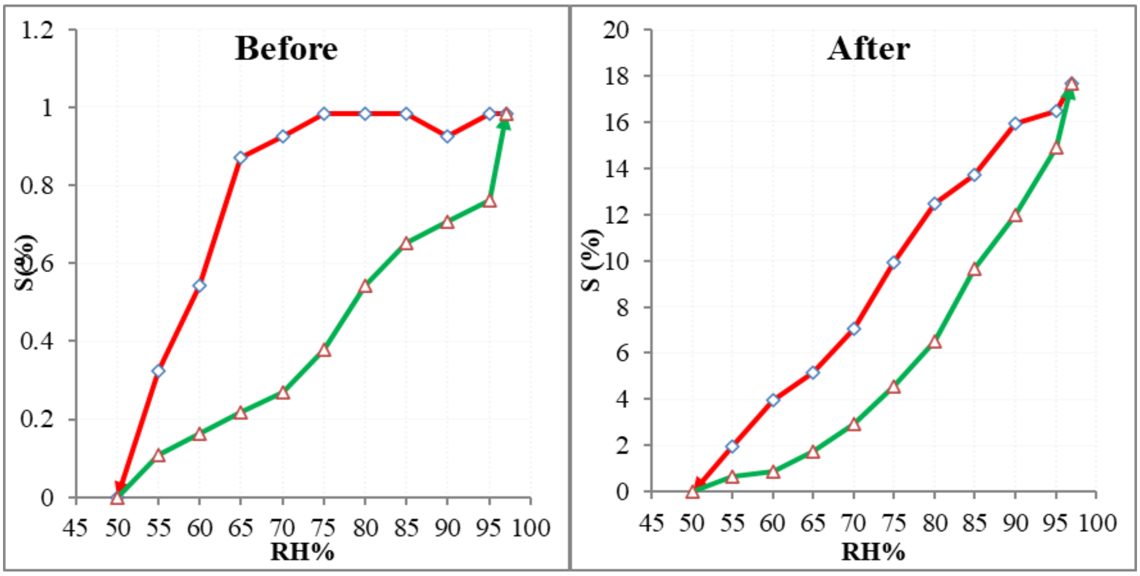

Figure 13: Humidity sensing variation of the Cr:Se sensor with humidity.

4. Conclusions

The results concluded that it is possible to manufacture thin films with a Cr:Se core-shell nanostructure using chemical synthesis. The XRD analysis revealed that the crystallinity increases when exposed to DBD plasma. The TEM measurements validated the core-shell structure of the sample. The expansion of the energy gap from 2.77 to 3.88 eV has confirmed the formation of the Cr:Se core-shell structure. Based on the findings, core-shell nanoparticles are promising for use in sensors and the medical field.

Acknowledgements

The authors would like to thank the University of Baghdad, College of Science, Department of Physics for their assistance in carrying out this work.

Conflict of interest

Authors declare that they have no conflict of interest.

Reference

1. A. Zaleska-Medynska, M. Marchelek, M. Diak, and E. Grabowska, Adv. Coll. Inter. Sci. **229**, 80 (2016). DOI: 10.1016/j.cis.2015.12.008.
2. B. R. Cuenya, Thin Sol. Fil. **518**, 3127 (2010). DOI: 10.1016/j.tsf.2010.01.018.
3. G. Merga, R. Wilson, G. Lynn, B. H. Milosavljevic, and D. Meisel, J. Phys. Chem. C **111**, 12220 (2007). DOI: 10.1021/jp074257w.
4. A. S. M. Aljaloud, A. F. Qasrawi, and L. H. K. Alfhaid, Optik **292**, 171395 (2023). DOI: 10.1016/j.ijleo.2023.171395.
5. J. Wang, Y. Xiang, W. Zhang, Y. Zhang, Q. Zhao, J. Li, and G. Liu, Fuel **351**, 128827 (2023). DOI: 10.1016/j.fuel.2023.128827.
6. A. Sobhani and M. Salavati-Niasari, J. Nanostruct. **7**, 141 (2017). DOI: 10.22052/jns.2017.02.008.
7. A. Abdelouas, W. L. Gong, W. Lutze, J. A. Shelnutt, R. Franco, and I. Moura, Chem. Mat. **12**, 1510 (2000). DOI: 10.1021/cm990763p.
8. M. Z. Liu, S. Y. Zhang, Y. H. Shen, and M. L. Zhang, Chinese Chem. Lett. **15**, 1249 (2004).
9. Y. Shin, J. M. Blackwood, I.-T. Bae, B. W. Arey, and G. J. Exarhos, Mat. Lett. **61**, 4297 (2007). DOI: 10.1016/j.matlet.2007.01.091.
10. V. Kuzmiak, V. Kolinsky, and K. Zdansky, in 2009 11th International Conference on Transparent Optical Networks (Ponta Delgada, Portugal IEEE, 2009). p. 1.
11. U. Hohenester and A. Trugler, IEEE J. Select. Top. Quant. Elect. **14**, 1430 (2008). DOI: 10.1109/JSTQE.2008.2007918.
12. W. D. Rappaport, G. C. Hunter, R. Allen, S. Lick, A. Halldorsson, T. Chvapil, M. Holcomb, and M. Chvapil, American J. Surg. **160**, 618 (1990). DOI: 10.1016/S0002-9610(05)80757-3.
13. M. S. Mohammed, B. H. Adil, A. S. Obaid, and A. M. Al-Shammari, Mat. Sci. For. **1050**, 51 (2022). DOI: 10.4028/www.scientific.net/MSF.1050.51.
14. A. Dehno Khalaji, Nanochem. Res. **6**, 18 (2021). DOI: 10.22036/ncr.2021.01.003.
15. F. Jiang, W. Cai, and G. Tan, Nanoscal. Res. Lett. **12**, 401 (2017). DOI: 10.1186/s11671-017-2165-y.
16. Z. N. Abdul-Ameer, Ibn AL-Haitham J. Pure Appl. Sci. **32**, 1 (2019). DOI: 10.30526/ 32.1.1974.
17. S. El-Nahas, M. S. A. El-Sadek, H. M. Salman, and M. M. Elkady, Mat. Chem. Phys. **258**, 123885 (2021). DOI: 10.1016/j.matchemphys.2020.123885.
18. M. O. Dawood, S. S. Chiad, A. J. Ghazai, N. F. Habubi, and O. M. Abdulmunem, AIP Conf. Proc. **2213**, 020102 (2020). DOI: 10.1063/5.0000136.
19. A. L. Andrady, S. H. Hamid, X. Hu, and A. Torikai, J. Photochem. Photobio. B Bio. **46**, 96 (1998). DOI: 10.1016/S1011-1344(98)00188-2.
20. J. Tauc, Mat. Res. Bullet. **3**, 37 (1968). DOI: 10.1016/0025-5408(68)90023-8.
21. A. Niema, E. Abbas, and N. Abdalameer, Dig. J. Nanomat. Biostruct. **16**, 1479 (2021). DOI: 10.15251/djnb.2021.164.1479.
22. N. Agmon, Chem. Phys. Lett. **244**, 456 (1995). DOI: 10.1016/0009-2614(95)00905-J.
23. R. Muneeb Ur, G. Shah, A. Ullah, R. Zia Ur, M. Arshad, R. Khan, Zulfiqar, B. Ullah, and I. Ahmad, J. Mat. Sci. Mat. Elect. **31**, 3557 (2020). DOI: 10.1007/s10854-020-02904-y.
24. C. Ma, A. Nikiforov, D. Hegemann, N. De Geyter, R. Morent, and K. Ostrikov, Int. Mat. Rev. **68**, 82 (2023). DOI: 10.1080/09506608.2022.2047420.
25. M. Avram, A. M. Avram, A. Bragaru, A. Ghiu, and C. Iliescu, Romanian J. Info. Sci. Tech. **11**, 409 (2008). DOI: 10.1109/SMICND.2007.4519654.
26. W. Li, J. Liu, C. Ding, G. Bai, J. Xu, Q. Ren, and J. Li *Fabrication of Ordered SnO2 Nanostructures with Enhanced Humidity Sensing Performance*. Sensors, 2017. **17**, 2392 DOI: 10.3390/s17102392.
27. I. Hotovy, J. Huran, P. Siciliano, S. Capone, L. Spiess, and V. Rehacek, Sens. Actuat. B Chem. **103**, 300 (2004). DOI: 10.1016/j.snb.2004.04.109.

دراسة تأثير البلازما غير الحرارية على الخصائص التركيبية والبصرية وحساسة الرطوبة لأغشية Cr:Se الرقيقة

تغريد احمد عبد الرزاق حلمي[1] ورامز احمد الانصاري[1]

[1]قسم الفيزياء، كلية العلوم للبنات، جامعة بغداد، بغداد، العراق

الخلاصة

على مدى السنوات القليلة الماضية، كان هناك تركيز كبير على دراسة تخليق وتطبيقات الجسيمات النانوية المعدنية. تمتلك هذه الجسيمات الصغيرة خصائص مميزة تميزها عن المعادن الكتلية. قشرة نواة Cr:Se تم تحضير أفلام نانوية بنسبة 6:4 باستخدام نفاثات البلازما، وتم ترسيبها باستخدام التحلل الحراري بالرش الكيميائي بسمك 158.9 نانومتر. تم تحليل الأفلام النانوية الرقيقة باستخدام حيود الأشعة السينية

(XRD)، والمطياف فوق البنفسجي (UV)-visible، والمجهر الإلكتروني الناقل (TEM). تدرس هذه الدراسة التركيب والخصائص البصرية لجزيئات النانو ذات القشرة النواة المصنوعة بنسب (6:4) من الكروم والسيلينيوم (Cr:Se). أنماط حيود الأشعة السينية تؤكد الطبيعة البلورية للجسيمات النانوية بالنسبة للنسبة متعددة البلورات. (6:4). تعريض أفضل بلورات البلازما غير الحرارية (تفريغ الحاجز العازل ((DBD) يؤدي إلى تغييرات كبيرة في حيود الأشعة السينية(XRD)، مما ينتقل نحو مرحلة أكثر بلورية. (31-57). تكشف مخططات تاوك عن اتجاه غير خطي في طاقات فجوة النطاق المباشر، مما يشير إلى زيادة كبيرة في الطاقة بين(2.77 ev و3.88). تحليل المجهر الإلكتروني الناقل يبرز تحسين توزيع الجسيمات النانوية وانتظامها. تُبرز هذه النتائج إمكانيات جزيئات Cr:Se النانوية للتقنيات البصرية والإلكترونية المتقدمة وأجهزة الاستشعار، بالإضافة إلى مجموعة متنوعة من التطبيقات التكنولوجية.

الكلمات المفتاحية: Cr:Se الجسيمات النانوية، قشرة نواة، الغلاف الأساسي، الخصائص البصري، الرطوبة.